

MASTERARBEIT

Zur Erlangung des akademischen Grades Master of Science.

Humboldt Universität Berlin, Institut für Physik

Erstgutachter: I.M. Sokolov Zweitgutachter: M. Falcke

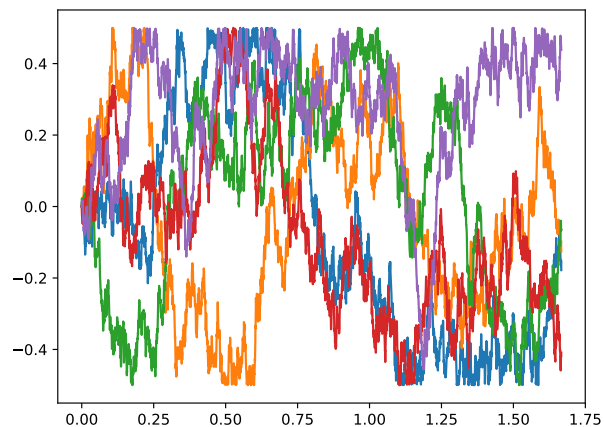
THEMA DER ARBEIT:

Simulation von verallgemeinerten Langevin Gleichungen mittels Kac-Zwanzig Wärmebad

eingereicht von: eingereicht am:

**MASTERARBEIT: SIMULATION VON VERALLGEMEINERTE
LANGEVIN GLEICHUNGEN MITTELS KAC-ZWANZIG
WÄRMEBAD**

MAXIMILIAN NOWOTTNICK



Simulation of generalized Langevin equations via a Kac-Zwanzig heat bath

April 2019

ABSTRACT

In this work we simulate generalized Langevin equations of the sub-diffusive type by explicit coupling of a particle to a oscillator heat bath. The advantage of this method is that the resulting model

is strictly deterministic and can be easily applied to hard-core environments. We then test this method in one dimensional closed intervals with reflecting boundaries and the two dimensional Lorentz gas.

ZUSAMMENFASSUNG

In dieser Arbeit simulieren wir verallgemeinerte Langevin Gleichungen der subdiffusiven Art durch explizite Kopplung eines Teilchens an ein Wärmebad aus Oszillatoren. Diese Methode resultiert dann in einer strikt deterministischen Dynamik, welche wir auf Geometrien mit hard-core Potentialen anwenden. Wir testen das Verfahren dann in Geometrien aus eindimensionalen Intervallen mit reflektierenden Wänden und dem zweidimensionalem Lorentzgas.

CONTENTS

I THE MODEL

| | | |
|-------|--|----|
| 1 | INTRODUCTION TO THE MODEL | 3 |
| 1.1 | Motivating the problem | 3 |
| 1.2 | The (generalized) Langevin Equation | 5 |
| 1.2.1 | The ohmic free behavior | 6 |
| 1.2.2 | The sub-Ohmic case | 7 |
| 1.3 | The Ford - Kac - Zwanzig- model | 8 |
| 1.4 | Comments on different variants of the oscillator Heat Bath | 10 |
| 1.5 | Setting the bath parameters | 17 |

II IMPLEMENTATION

| | | |
|-------|--|----|
| 2 | THE ALGORITHM | 23 |
| 2.1 | The velocity Verlet method | 23 |
| 2.1.1 | Impulsive Verlet | 24 |
| 2.2 | Testing the model | 25 |
| 2.2.1 | The free behaviour | 26 |
| 2.3 | Testing the reflecting case | 30 |
| 2.3.1 | Testing on a 1-d box | 30 |
| 2.3.2 | Testing on a 2-d lattice of spheres | 32 |
| 2.3.3 | summing it up | 33 |
| 3 | SIMULATION RESULTS | 35 |
| 3.1 | simulation in a 2-d lattice of spheres | 35 |
| 3.1.1 | Results in the ohmic case | 36 |
| 3.1.2 | Results in the subohmic case | 38 |
| 3.2 | particle in a 1-d box | 38 |

III APPENDIX

| | |
|--------------|----|
| BIBLIOGRAPHY | 47 |
|--------------|----|

LIST OF FIGURES

- Figure 1.1 Comparison log-log plot of kernel approximation between rectangle and Simpson scheme. 1000 terms are used in the sum approximation of the kernel $K(t) = t^{-0.6}$. [20](#)
- Figure 2.1 MSD for different bath sizes in the $\alpha = 1$ case and two dimensions . Averages taken over 1000 simulations. [27](#)
- Figure 2.2 Results for the free integration case for $\alpha = 1$. $N = 5000$ bath particles used and simulated in 2 dimensions. [28](#)
- Figure 2.3 Results for the free integration case for $\alpha < 1$. All Plots are averages over 1000 simulations at $T = 100K$. [29](#)
- Figure 2.4 log-log plots of MSD versus time. The arrows indicate the expected slopes 0.8, 0.6 and 0.4 for easier comparison by eye. The bath sizes are 14k, 21k and 40k. [29](#)
- Figure 2.5 Results for the box with reflecting boundaries. All plots are averages over 1000 simulations at $T = 100K$. Times are rescaled by $t_E = 800s$ and lengths by $L = \sqrt{2D_\alpha t_E^\alpha}$ for easier reading. Figure [2.5a](#) shows three example plots of the particle position as a function of time for the ohmic case, figure [2.5b](#) for the $\alpha = 0.8$ case. The bath size is $N = 14k$. [31](#)
- Figure 2.6 Results for the box with reflecting boundaries. Energy plots are averages over 1000 simulations at $T = 100K$. Times will be rescaled by $t_E = 800s$ and lengths by $L = \sqrt{2D_\alpha t_E^\alpha}$ for easier reading. D_α is the expected diffusion coefficient for the infinite bath as derived in chapter one. Figure [2.6a](#) shows 500 example plots of the particle x - position as a function of the particle y - position for the ohmic case, figure [2.6b](#) for the $\alpha = 0.8$ case. [33](#)
- Figure 3.1 MSD for different sphere concentrations ϕ together with linear fits. All simulations for 14k bath particles at 100K temperature. All times have been rescaled by the lattice scale time $t_E = 3000s$, all MSD by the squares lattice constant L^2 . [37](#)

- Figure 3.2 plot of relative coefficients of diffusion $D'(\phi) = \frac{D(\phi)}{D(0)}$ as functions of volume fraction ϕ , from our fits of the heat bath simulation and the Langevin simulation, as well as according to equation 3.1 38
- Figure 3.3 $\alpha = 0.8$ plots. Figure ref 3.4a shows the linear fits of the MSD curves versus time, figure 3.4b the relative (generalized) coefficients of diffusion 39
- Figure 3.4 Plot of the bin probabilities for $\alpha = 1$ rescaled by the box lengths L . figure 3.5a shows the behaviour at $t = 1s, 10s, 5000s$, figure 3.5b at only the later two times for better visibility. 41
- Figure 3.5 Plot of the bin probabilities in the sub-ohmic case rescaled by the box lengths L . figure 3.6a shows the behaviour at $t = 1s, 10s, 5000s$. 42
- Figure 3.6 Plots of the probability density at simulation end for boxes of different lengths L' for $L' = \frac{L}{2}, \frac{L}{4}$ and $\frac{L}{8}$ compared to the length $L = 1.976 \cdot 10^{-2} m$, $t_E = 3000s$ of the previous tests. $\alpha = 0.8$ and 14k bath particles, all other parameters are as in figure 3.5. The probability density for $L' = \frac{L}{4}$ and $\frac{L}{8}$ have been lifted upward by $\frac{1}{100}$ and $\frac{2}{100}$ for easier reading. 43

LIST OF TABLES

- Table 1.1 Important bath parameters and values for the fully mobile bath, $\kappa = 1$ with uniform frequency distribution of spacing $\Delta\omega$. 20

Part I
THE MODEL

INTRODUCTION TO THE MODEL

Since the seminal work by A. Einstein [3], the field stochastic processes, random walks and diffusion has been applied to a broad field of subjects, including finance [2], neuroscience[13] and polymer physics[4]. Of special interest today are models exhibiting anomalous diffusion, that is models for which

$$\langle (x(t) - x(0)) \rangle \propto t^\alpha, \quad \alpha \neq 1$$

holds.

The general idea of this thesis is to model anomalous diffusion not via a specific type of stochastic differential equation, but with a strictly deterministic system approaching the stochastic equation in the thermodynamic limit. The random force and friction are the result of interactions with a 'heat bath', that is a large reservoir of particles interacting with the distinguished particle of interest at a sharply defined temperature.

This might at first seem like an unwieldy and impractical procedure, after all regular Langevin type stochastic differential integrations have known fast and accurate integration algorithms[16] and indeed it will turn out that for regular memory-less equations of this type the procedure presented here is comparatively labour intensive and slow. However, once we introduce 'long term memory', the precise meaning of which we will make clear in the following section, there is no standard procedure to our knowledge how to propagate these equations in the presence of hard core interactions (and even in the memory free case the topic is not wholly trivial), but there are already known algorithms how to deal with this situation in deterministic systems.

In that sense, the explicit heat bath will act as a bridge to allow the application of these methods to a stochastic system under consideration.

1.1 MOTIVATING THE PROBLEM

The probably most intuitive way to add random statistical interactions to a deterministic system is by simply adding a random force F_R to Newton's equation, $m\ddot{x} = F + F_R$. In order to satisfy known equilibrium statistical relations this force has to be accompanied by a friction term, so that at each time on average the same amount of en-

ergy is added and drained from the system once thermal equilibrium is reached. This idea is known as the Langevin equation formalism

$$m\ddot{x} = F - B\dot{x} + F_R$$

Without going into details yet, we want to show some problems that appear when simulating differential equations involving stochastic forces in combination with reflecting boundaries. For this we will look at a naive discrete integration scheme for the equation above.

$$\begin{aligned} y_{n+1} &= y_n + \dot{y}_n \Delta t \\ \dot{y}_{n+1} &= -B\dot{y}_n + A\sqrt{\Delta t} \cdot \text{rand}_{\text{gauss}}(0, 1) \end{aligned} \quad (1.1)$$

A, B are arbitrary positive parameters and Δt is the step size of the integration scheme. $\text{rand}_{\text{gauss}}(0, 1)$ is a Gaussian random number with mean zero and standard deviation one, re-sampled at each time step, so that consecutive steps have independent random forces $F_R(t_i) = A\sqrt{\Delta t} \cdot \text{rand}_{\text{gauss}, i}(0, 1)$, which do depend on $\sqrt{\Delta t}$ though. Now let us say that during a step n the position vector y arrives at a reflecting boundary at time $t_n + \frac{\Delta t}{2}$. An intuitive way of implementing this reflection is then to integrate the system forward in time until contact, reflect and integrate with reflected velocity for the remaining time step.

$$\begin{aligned} y_{n+\frac{1}{2}} &= y_n + \dot{y}_n \frac{\Delta t}{2} \\ \dot{y}_{n+\frac{1}{2}} &= -\dot{y}_{n+\frac{1}{2}} \\ \dot{y}_{n+\frac{1}{2}} &= -B\dot{y}_n + A\sqrt{\frac{\Delta t}{2}} \cdot [\text{rand}_{\text{gauss}}(0, 1) = m] \\ y_{n+1} &= y_{n+\frac{1}{2}} + \dot{y}_{n+\frac{1}{2}} \frac{\Delta t}{2} \\ \dot{y}_{n+1} &= -B\dot{y}_{n+\frac{1}{2}} + A\sqrt{\frac{\Delta t}{2}} \cdot m \end{aligned}$$

While this implementation might seem straight forward at first, it is important to note that the choice of the order of the first three equations was arbitrary, an equally intuitive choice would have been.

$$\begin{aligned} \dot{y}_{n+\frac{1}{2}} &= -B\dot{y}_n + A\sqrt{\frac{\Delta t}{2}} \cdot [\text{rand}_{\text{gauss}}(0, 1) = m] \\ y_{n+\frac{1}{2}} &= y_{n+\frac{1}{2}} + \dot{y}_{n+\frac{1}{2}} \frac{\Delta t}{2} \\ \dot{y}_{n+\frac{1}{2}} &= -\dot{y}_{n+\frac{1}{2}} \\ \dot{y}_{n+1} &= -B\dot{y}_{n+\frac{1}{2}} + A\sqrt{\frac{\Delta t}{2}} \cdot m \\ y_{n+1} &= y_{n+\frac{1}{2}} + \dot{y}_{n+1} \frac{\Delta t}{2} \end{aligned}$$

It is not at all clear that both implementations, that is reflecting the old or the updated velocity, lead to the same system behavior or what

if any the conditions on the parameters and step size are for both implementations to describe the same behavior. Another point of note is that both half steps in the schemes involve the same random force, that is the random number is drawn once and reused in the second half step. This essentially leads to a correlation time of the random force in the vicinity of the boundary. One might think that this problem is easily solved by simply redrawing the random numbers even for the half steps, but this carries with it another kind of problem. Let us for example say y reaches the boundary exactly at the end of a step Δt . In the second scheme that means that the system is essentially updated as the free system for the step and the velocity u inverted at the end. Now, we could just as easily have modeled the step as two half steps, but in this case when the random force is redrawn for the second half step it is most likely not the case that the boundary is reached at Δt , which at least casts doubt on the practice of inverting the velocity at a fixed time of contact.

We do not claim that these problems are insurmountable or that implementations that solve these questions do not already exist, just that these examples show that it is not straight forward to integrate this type of equation in the presence of hard reflecting boundaries. In any case, for equations of type 1.1 the physical behavior is known for a large variety of systems, so whatever scheme one comes up with, it is easy to verify the correctness of the scheme by comparison with known results.

However, the more general type of equation considered in this work

$$\begin{aligned} y_{n+1} &= y_n + \dot{y}_n \Delta t \\ \dot{y}_{n+1} &= - \int_0^{t_n} B(t_n - t') \dot{y}(t') dt' + \cdot \text{rand}(t_n, \cdot, y_0, \dots, y_n) \end{aligned}$$

Not only lacks such a body of results for comparison, the random force is now a function of all prior steps which multiplies the troubles and shows the need for a simulation scheme which circumvents these problems all together by not sampling from a random force, but using a deterministic force that behaves like the random one in the thermodynamic limit of the system modeled in this work.

1.2 THE (GENERALIZED) LANGEVIN EQUATION

This section will be a brief review of the aforementioned stochastic differential equation to be modeled, the generalized Langevin equations (GLE) in the sub diffusive case in d dimensions and its important properties (mean squared displacement MSD and correlation functions) contrasted with the regular Langevin equation. The GLE is an equation of the form:

$$m \frac{d}{dt} v = - \int_0^t K(t-t') v(t') dt' + \xi(t) + F(x)$$

with a memory kernel K and a random force ξ and a deterministic force F . The random force is a random process the with zero mean $\langle \xi(t) \rangle = 0$ at all times, hence the average of v depends only on the kernel $m \frac{d}{dt} \langle v \rangle = - \int_0^\infty \langle K(t-t') \rangle + F$, a regular equation of motion with a generalized friction term. To satisfy equilibrium statistical physics (for a bath at thermal equilibrium) the random force and the kernel have to be related by the fluctuation dissipation theorem

$$\langle \xi(t) \xi(t') \rangle = 2kT K(t-t')$$

For the kernel two cases are of interest in this work, the so called ohmic case describing memory less normal diffusion and the fractional Langevin equation case describing subdiffusion with algebraically decaying long term memory

$$\begin{aligned} K(t) &\propto \delta(t) \rightarrow \langle x^2(t) \rangle = 2dDt \\ K(t) &\propto t^{-\alpha} \rightarrow \langle x^2(t) \rangle \propto t^\alpha \quad \alpha \in (0, 1) \end{aligned}$$

1.2.1 The ohmic free behavior

The mean squared displacement (MSD) $\langle x^2(t) \rangle$ in the case of delta function like memory kernel,

$$K(t) = \gamma \cdot \delta(t)$$

in the literature of heat baths often called the Ohmic case (as the regular Ohm's law can indeed be modeled with this kind of equation) is well known[17] and has the form (in the case $x(0) = 0$ and without deterministic force)

$$\begin{aligned} \langle x^2(t) \rangle &= 2d \frac{kT}{\gamma} \left(t - \frac{m}{\gamma} + \frac{m}{\gamma} e^{-\frac{\gamma}{m}t} \right) \\ \langle x^2(t) \rangle &\sim d \frac{kT}{\gamma} t; t \rightarrow \infty \\ \langle x^2(t) \rangle &\sim 2d \frac{kT}{\gamma} \left(\frac{\gamma}{2m} t^2 \right) = \langle v^2(t) \rangle_{eq} t^2; t \rightarrow 0 \end{aligned}$$

Thus the MSD shows an exponential transition from a ballistic regime ($\langle x^2(t) \rangle$ grows as if $x = v \cdot t$ with constant velocity) and a diffusive regime with coefficient $D = \frac{kT}{\gamma}$ at times large compared to $(\frac{m}{\gamma})$. The velocity correlation function similarly shows an exponential decay of fluctuation towards thermal equilibrium.

$$\langle v(t) v(t') \rangle = d \frac{kT}{m} e^{-\frac{\gamma}{m}|t-t'|}$$

Thus the memory-less case models regular diffusion $\langle x^2(t) \rangle = 2dDt$. In this case the model could also be described by a Fokker Planck equation or a continuous time random walk with appropriate jump rates and distribution of jump lengths and this 'overlap' of the three ways to model the system also holds in the presence of a deterministic force. In contrast, when the long term memory case is under consideration, the continuous time random walk can still be mapped to a generalized Fokker Planck equation, but there is now known correspondence between these two and a GLE for arbitrary forces.

1.2.2 The sub-Ohmic case

The long term memory or sub-ohmic case will exhibit sub-diffusive long term behaviour at long times and will be the model under consideration in this thesis. For the free case, the moments of the relevant quantities are known [7] and can be readily obtained via the Laplace transform. The kernel is now determined by two parameters, a constant of proportionality and α , the exponent of the memory decay $K(t) = \gamma_\alpha t^{-\alpha}$. This kernel relates the total history to the generalized friction term and gives a hint of the problems that arise in the numerical integration of these equations, since each step forward in time depends on all prior steps.

Since the main results are most conveniently expressed in terms of generalized Mittag Leffler functions [6](MLF), we will briefly introduce them here. MLF are generalised exponential functions, the faculty in the denominators in the Taylor series expressed as the continuous interpolation of the faculty, the Gamma function $\Gamma(n) = n!$ and then shifted by a real number v and rescaled by another β . In formula these are then

$$\begin{aligned} E_{\beta,v}(x) &= \sum_0^{\infty} \frac{x^n}{\Gamma(\beta n + v)} \\ E_v(x) &= \sum_0^{\infty} \frac{x^n}{\Gamma(n + v)} = E_{1,v}(x) \end{aligned}$$

The long term asymptotics are known and are

$$E_{\beta,v}(x) \sim \frac{x^{-1}}{\Gamma(v - \beta n)} ; \quad x \rightarrow \infty$$

The main results for the free sub-ohmic behaviour are then[6]

$$\begin{aligned} \langle x^2(t) \rangle &= 2 \frac{kT}{m} E_{\alpha+2,3} t^2 (-\gamma_\alpha t^{-\alpha+2}) \\ \langle x^2(t) \rangle &\propto t^\alpha ; t \rightarrow \infty \\ \langle x^2(t) \rangle &\propto t^2 ; t \rightarrow 0 \end{aligned}$$

Thus, for $0 < \alpha < 1$ this model describes subdiffusion at long times. Though there exist sub-diffusive generalisations of Fokker Planck equations, there is no known way to relate these to this GLE for arbitrary external forces. Since there is a wealth of literature on the behaviour of these in hard core geometries but very little known about the GLE behaviour in these circumstances, this motivates our exploration of the numerical integration scheme presented in the next section.

1.3 THE FORD - KAC - ZWANZIG- MODEL

The following overview will mostly follow Zwanzig [17]. The Ford-Kac-Zwanzig model (ZM) is a model of a single particle coupled to many harmonic oscillators. The oscillators do not interact with each other except through their shared coupling to the single distinguished particle. If the oscillators initial values are distributed according to a Boltzmann-Distribution, they act as a heat bath interacting with the distinguished particle in the limit of infinite oscillators. The coupling constants can be chosen to facilitate a wide range of different interactions between particle and bath, among them the coupling to a ohmic heat bath (OHB), that is an interaction in which the bath gives rise to a constant drag coefficient. In particular, in the OHB case analytic solutions to the model can be derived, so the model serves as a good starting point for the exploration of how dissipation and Langevin dynamics emerge through the conservative interaction of many particles. In formula the model is characterized as follows:

$$\begin{aligned}\dot{x}_i &= \frac{p_i}{M} \\ \dot{p}_i &= -\sum_j \left(\frac{\gamma_j^2}{\omega_j^2} \right) x_i + \sum_j \gamma_j q_{j,i} \\ \dot{q}_{k,i} &= r_{k,i} \\ \dot{r}_{k,i} &= -\omega_k^2 q_{k,i} + \gamma_k x_i\end{aligned}$$

here \vec{x} , \vec{p} are coordinate and impulse vector of the heavy particle, \vec{r}_j , \vec{p}_j the coordinate and impulse of the j -th oscillator. The j -th oscillator is coupled to the particle with coupling constants γ_j and has a frequency of ω_j . All oscillator masses are set to one. Since the coupling to the particle is linear, the system can be solved partially (with respect to the initial values of the bath) by integrating the bath equations, though explicit calculations will be provided later for a slightly more general model and we will only look at some important results. The model can be shown to lead to a resulting equation of motion for the distinguished particle that has the following form

$$\begin{aligned}\dot{P} &= - \sum_k \gamma_k \left(\left(q_{k,i}(0) - \frac{\gamma_k}{\omega_k^2} x(0) \right) \cos \omega_k t + \frac{p_{k,i}(0)}{\omega_k} \sin \omega_k t \right. \\ &\quad \left. - \gamma_k \int_0^t \frac{p(s)}{M} \frac{\cos \omega_k(t-s)}{\omega_k^2} ds \right)\end{aligned}$$

This result formally has the structure of a GLE equation, $\dot{P} = \int_0^t K(t-s) \frac{p(s)}{M} ds + F_r(t)$ with memory kernel:

$$K(t) = \sum_k \gamma_k^2 \frac{\cos \omega_k(t-s)}{\omega_k^2}$$

and random force:

$$F_r(t) = - \sum_k \gamma_k \left(\left(q_{k,i}(0) - \frac{\gamma_k}{\omega_k^2} x(0) \right) \cos \omega_k t + \frac{p_{k,i}(0)}{\omega_k} \sin \omega_k t \right)$$

. Indeed, if the initial distributions of the bath are chosen randomly from a Boltzmann distribution, one can see by averaging over all possible initial values

$$\begin{aligned}\langle F_r(t) \rangle &= 0 \\ \langle F_r(t) F_r(s) \rangle &= 2kT K(t-s)\end{aligned}$$

So the term indeed models a random force of zero mean and satisfying a the fluctuation dissipation relation. In the case of infinitely many oscillators with sufficiently densely distributed frequencies one can further simplify the kernel as an approximation to a fourier transform

$$\begin{aligned}K(t) &= \sum_k \gamma_k^2 \frac{\cos \omega_k(t-s)}{\omega_k^2} \\ &\propto \int g(\omega) \frac{\gamma^2(\omega)}{\omega_k^2} \cos \omega(t-s) d\omega\end{aligned}$$

By choosing different distributions for the frequencies $g(\omega)$ and the coupling constants a wide array of GLE equations can be modeled via a deterministic Hamiltonian (though with random initial conditions), the OHB case corresponds to $K(t) = \Gamma \delta(t)$ with drag coefficient Γ and g is the the distribution density of the frequencies. In [17] the case is implemented by choosing constant coupling coefficients and a quadratic distribution, but in this thesis a different setup will be chosen, which follows in analogy to [9]

In this sense the ZM provides a theoretic justification for the use of the Langevin formalism. However in this work we will be using it as a practical tool to simulate GLE, since there is currently no clear consensus on how to simulate GLE with hard core interactions, but there is a wealth of literature how to integrate deterministic systems with these interactions.

1.4 COMMENTS ON DIFFERENT VARIANTS OF THE OSCILLATOR HEAT BATH

The fact that the model in the thermodynamic limit with kernel $K(t) = K_0 t^{-\alpha}$ behaves like the GLE corresponding to said kernel has been proven mathematically by Kupferman[9]. However, Kupferman has chosen a bath Hamiltonian that subtly differs from the original ZM and we will call this special case of the model the mobile bath (MB). The Hamiltonians describing these models are (now with explicit bath masses)

$$\begin{aligned}
 H_{ZM} &= \frac{p^2}{2M} + \sum_j \frac{p_j^2}{2m_j} + \sum_j \frac{\omega_j^2}{2} \left(q_j - \frac{\gamma_j}{\omega_j^2} X \right)^2 \\
 &= \frac{p^2}{2M} + \sum_j \frac{p_j^2}{2m_j} + \sum_j \left(\frac{\omega_j^2}{2} q_j^2 - \gamma_j q_j X + \frac{\gamma_j^2}{2\omega_j^2} X^2 \right) \\
 &= \frac{p^2}{2M} + \sum_j \frac{p_j^2}{2m_j} \\
 &\quad + \sum_j \left(\frac{\gamma_j^2}{2\omega_j^2} (q_j - X)^2 - \frac{\gamma_j^2}{2\omega_j^2} q_j^2 + \frac{\gamma_j^2}{\omega_j^2} q_j X + \frac{\omega_j^2}{2} q_j^2 - \gamma_j q_j X \right) \\
 &= \frac{p^2}{2M} + \sum_j \frac{p_j^2}{2m_j} \\
 &\quad + \sum_j \left(\frac{\gamma_j^2}{2\omega_j^2} (q_j - X)^2 + \frac{1}{2} \left(\omega_j^2 - \frac{\gamma_j^2}{\omega_j^2} \right) q_j^2 + \left(\frac{\gamma_j^2}{\omega_j^2} - \gamma_j \right) q_j X \right) \\
 H_{MB} &= \frac{p^2}{2M} + \sum_j \frac{p_j^2}{2m_j} + \sum_j \frac{k_j}{2} (q_j - X)^2
 \end{aligned}$$

As we can see by factoring out the Bath potential, the ZM consists of harmonic coupling between bath particles and an distinguished particle as well as an additional coupling to the coordinate origin and a term $\propto \sum q_j X$. The coupling constants for these three contributions are determined by the γ_j and the frequencies ω_j and are not independent from each other. The MB on the other hand only has a harmonic coupling between bath particles and the distinguished particle. The models are the same for one particular choice of constants, namely $\omega_j^2 = \gamma_j$.

Though it might not be immediately obvious, both models result in the same diffusion type (for the appropriate choice of constants in each case). To avoid confusion from citing results for these models individually, we will use our own notation and slightly more general

model.¹. The model will contain both the MB and the ZM as special cases and thus provide a convenient way of translating the appropriate choices of constants from one model to another. This model will be called generalised Kac-Zwanzig-model (GZM), it will contain a bath coupling to the origin via springs S_j and the distinguished particle with springs s_j

$$\begin{aligned} H_{GZM} &= U + \frac{P^2}{2M} + \sum_j \frac{p_j^2}{2m_j} + \sum_j \frac{S_j}{2} q_j^2 + \sum_j \frac{s_j}{2} (q_j - X)^2 \\ &= U + \frac{P^2}{2M} + \sum_j \frac{p_j^2}{2m_j} + \sum_j \frac{S_j}{2} q_j^2 + \sum_j \frac{s_j}{2} (q_j^2 - 2q_j X + X^2) \\ &= U + \frac{P^2}{2M} + \sum_j \frac{p_j^2}{2m_j} + \sum_j \frac{(S_j + s_j)}{2} q_j^2 + \sum_j \frac{s_j}{2} X^2 - \sum_j s_j q_j X \end{aligned}$$

the effective coupling constant of the bath to the origin is $S_j + s_j = k_j$, the frequency of these oscillators hence $\omega_j = \sqrt{\frac{k_j}{m_j}}$. It will be further convenient to have a dimensionless measure of the relative contributions to that coupling, $\kappa_j = \frac{s_j}{S_j + s_j}$

$$\begin{aligned} H_{GZM} &= U(X) + \frac{P^2}{2M} + \sum_j \frac{p_j^2}{2m_j} + \sum_j \frac{k_j}{2} q_j^2 + \sum_j \frac{k_j \kappa_j}{2} X^2 - \sum_j k_j \kappa_j q_j X \\ &= U(X) + \frac{P^2}{2M} + \sum_j \frac{p_j^2}{2m_j} + \sum_j \frac{k_j}{2} (q_j - \kappa_j X)^2 + \sum_j \frac{k_j}{2} (\kappa_j - \kappa_j^2) X^2 \end{aligned}$$

In this way we can see that the MB case is realized for $\kappa = 1$. In a first step we will show that the model can be made to behave according to a GLE in the thermodynamic limit by retracing the steps for ZM in [17]. The idea is to partially integrate out the equations of motion for the bath as if we already knew the trajectories of the distinguished particle and then use the linear form of the coupling to substitute the obtained bath solutions back into the equation for the distinguished particle.

The equations of motion are

¹ The derivation that follows as well as subsequent ruminations on the appropriate bath size is largely due to discussions with Prof. I. M. Sokolov.

$$\begin{aligned}
\dot{P} &= -U(X)' - \sum_j^N k_j \kappa_j X + \sum_j k_j \kappa_j q_j \\
&= -U(X)' - \sum_j m_j \omega_j^2 \kappa_j X^2 - \sum_j m_j \omega_j^2 \kappa_j q_j X \\
\dot{X} &= \frac{P}{M} \\
\dot{p}_j &= -k_j q_j + k_j \kappa_j X \\
&= -m_j \omega_j^2 q_j^2 + m_j \omega_j^2 \kappa_j X \\
q_j &= \frac{p_j}{m_j}
\end{aligned}$$

The Equation for the bath momenta have known general solutions in dependence of the still unknown $X(t)$. By partial integration, this solution will then be brought in an form that is expressedly linearly dependent on $X(0)$ and can then be substituted back in the equation for the distinguished particle

$$\begin{aligned}
q_j &= q_j(0) \cos \omega_j t + q_j(0) \frac{\sin \omega_j t}{\omega_j} + \kappa_j \omega_j \int_0^t \frac{X(t') \sin \omega_j (t-t')}{\omega_j} dt' \\
&= q_j(0) \cos \omega_j t + q_j(0) \frac{\sin \omega_j t}{\omega_j} \\
&\quad + \kappa_j \omega_j \left(\frac{X(t)}{\omega_j} - \frac{X(0) \cos \omega_j t}{\omega_j} - \int_0^t \frac{\dot{X}(t') \cos \omega_j (t-t')}{\omega_j} dt' \right) \\
&= (q_j(0) - \kappa_j X(0)) \cos \omega_j t + q_j(0) \frac{\sin \omega_j t}{\omega_j} \\
&\quad + \kappa_j X(t) - \kappa_j \int_0^t \dot{X}(t') \cos \omega_j (t-t') dt' \\
\dot{P} &= -U' - \sum_j^N k_j \kappa_j X + \sum_j k_j \kappa_j q_j \\
&= -U' - \sum_j^N k_j \kappa_j X + \sum_j k_j \kappa_j \left((q_j(0) - \kappa_j X(0)) \cos \omega_j t + q_j(0) \frac{\sin \omega_j t}{\omega_j} \right) \\
&\quad + \sum_j k_j \kappa_j^2 X(t) + \sum_j k_j \kappa_j^2 \int_0^t \dot{X}(t') \cos \omega_j (t-t') dt'
\end{aligned}$$

A curious feature in the model is now apparent, the distinguished particle experiences an effective force $\tilde{U}'(X) = U'(X) - \sum_j k_j (\kappa_j - \kappa_j^2) X$ that differs for all choices of coupling except the mobile bath, which is therefore a convenient choice of coupling parameters. Now the result

will be ordered in a way that formally resembles a GLE which will then be shown to behave like one for appropriate initial conditions.

$$\begin{aligned}\dot{P} &= -\tilde{U}'(X) - \int_0^t \dot{X}(t') K(t-t') dt' + F_R & (1.2) \\ K(t) &= \sum_j k_j \kappa_j^2 \cos \omega_j t \\ F_R &= \sum_j k_j \kappa_j \left((q_j(0) - \kappa_j X(0)) \cos \omega_j t + q_j(0) \frac{\sin \omega_j t}{\omega_j} \right)\end{aligned}$$

With memory kernel K and random force F_R .

Now, for sufficiently dense distributions of bath frequencies, the kernel can be seen as a sum approximation to a (cosine-) Fourier transform involving the spectral density $g(\omega) = \frac{dN(\omega)}{d\omega}$ with $N(\omega)$ being the number of oscillators of frequency $\leq \omega$.

$$K(t) \approx \int_0^\infty g(\omega) k(\omega) \kappa^2(\omega) \cos \omega t d\omega \quad (1.3)$$

And hence by choosing the right frequency distribution and coupling constants this term can approximate any desired generalised friction term. The term F_R can be made to behave like a random force by choosing the initial conditions for the bath as the thermal state, that is by drawing the initial distribution randomly from the corresponding Boltzmann distributions. Fixing $X(0) = 0$

$$\begin{aligned}q_j(0) &= n_{q,j} \sqrt{\frac{kT}{2m_j}} \\ p_j(0) &= n_{p,j} \sqrt{\frac{kT m_j}{2\omega_j^2}}\end{aligned}$$

With random numbers $n_{q,j}, n_{p,j}$ distributed i.i.d according to the Gaussian distribution \mathcal{N}_{01} . It is immediately clear that the force is a sum of random numbers with zero mean, that is $\langle F_R(t) \rangle = 0$. The correlation function can also be calculated and behaves like one expects from a GLE.

From the equipartition theorem in d dimensions, that is $\left\langle \frac{p_j^2}{2m_j} \right\rangle = \left\langle m_j \omega_j^2 \frac{q_j^2}{2} \right\rangle = \frac{d k T}{2}$ and by using some elementary trigonometric relations as well as the fact that all random numbers are uncorrelated we can see that

$$\begin{aligned}
\langle F_r(t) F_r(t') \rangle &= \sum_{i,j} k_i k_j \kappa_i \kappa_j \left\langle \left((q_i(0)) \cos \omega_i t + \frac{p_i}{m_i}(0) \frac{\sin \omega_i t}{\omega_i} \right) \right. \\
&\quad \cdot \left. \left((q_j(0)) \cos \omega_j t' + \frac{p_j}{m_i}(0) \frac{\sin \omega_j t'}{\omega_j} \right) \right\rangle \\
&= \sum_i k_i \kappa_i^2 \left(\langle m_i \omega_i^2 q_i(0) \rangle^2 \cos \omega_i t \cos \omega_i t' + \dots \right. \\
&\quad \left. \left\langle \frac{p_i^2}{m_i}(0) \right\rangle \sin \omega_i t \sin \omega_i t' \right) \\
&= kT \sum_i k_i \kappa_i^2 \cos \omega_i (t - t') \\
&= kTK(t - t')
\end{aligned}$$

So our random force fulfills the fluctuation dissipation relation expected of an GLE. In that sense, our model can be seen as a deterministic system who's properties when averaging over the initial thermal distribution is described by the GLE we want to examine. The next step is to look at the diffusion coefficient and scaling of the model for the kernels we will be using in the rest of this thesis, kernels that decay algebraically

$$K(t) = \gamma_\alpha t^{-\alpha} \quad \alpha \in (0, 1)$$

We start at equation 1.2 and apply a Laplace transform. Setting $X(0) = 0$:

$$\begin{aligned}
M\ddot{X}(t) &= - \int_0^t \dot{X}(t') K(t-t') dt' + F_R(t) \\
M(-V(0) + s^2 X(s)) &= sX(s) K(s) + F_R(s) \\
X(s)(Ms^2 + sK(s)) &= F_R(s) + MV(0) \\
X(s) &= \frac{1}{Ms^2 + sK(s)} (F_R(s) + MV(0)) \\
&= H(s) (F_R(s) + MV(0))
\end{aligned}$$

Or transformed back $X(t) = \int_0^t (F_R(t) H(t-t') + MV(0) H(t')) dt'$.

Accordingly

$$\begin{aligned}
 \langle X^2(t) \rangle &= \left\langle \int_0^t (H(t-t') (F_R(t')) dt' + M V(0) H(t)) \right. \\
 &\quad \cdot \left. \int_0^t (H(t-t'') (F_R(t'')) dt'' + M V(0) H(t)) \right\rangle dt' dt'' \\
 &= \int_0^t H(t-t') \int_0^t H(t-t'') \langle F_R(t') F(t'') \rangle dt' dt'' \quad (1.4) \\
 &\quad + \langle M V^2(0) \rangle H^2(t)
 \end{aligned}$$

We used the fact that the random force is uncorrelated to the initial velocity and has zero mean to vanish the cross terms. The term involving the force correlations will be examined in the Laplace domain using the fluctuation dissipation theorem.

$$\begin{aligned}
 \int_0^t H(t-t') \int_0^t H(t-t'') \langle F_R(t') F(t'') \rangle dt'' dt' &= 2k_b T \int_0^t H(\xi) \cdot \left(\int_0^t H(\eta) K(\xi-\eta) d\eta \right) d\xi \\
 \mathcal{L} \left(\int_0^t H(\eta) K(\xi-\eta) d\eta \right) &= H(s) K(s) \\
 &= \frac{K(s)}{Ms^2 + sK(s)} \\
 &= \frac{1}{\frac{M}{K(s)}s^2 + s} \\
 &= \frac{1}{s \left(\frac{M}{K(s)}s + 1 \right)} \\
 &= \frac{1}{s} - \frac{M}{Ms + K(s)} \\
 &= \frac{1}{s} - MsH(s) \\
 \hookrightarrow \left(\int_0^t H(\eta) K(\xi-\eta) d\eta \right) &= -M\dot{H}(t) + H(0) + 1
 \end{aligned}$$

Now $H(0) = \lim(s \rightarrow \infty) H(s) = 0$, so that finally it follows:

$$\begin{aligned}
\int_0^t H(t-t') \int_0^t H(t-t'') \langle F_R(t') F(t'') \rangle dt'' dt' &= V \int_0^t H(t') (-M \dot{H}(t') + 1) dt' \\
&= 2k_b T M \int_0^t \frac{d}{dt'} \frac{H^2(t')}{2} dt' + \dots \\
&\dots 2k_b T \int_0^t H(t') dt' \\
&= -k_b T M H^2(t) + 2k_b T \int_0^t H(t') dt' \\
\langle X^2(t) \rangle &= 2k_b T \int_0^t H(t') dt'
\end{aligned}$$

In the last equation a thermalised initial condition $MV^2(0) = k_b T$ was assumed when adding the terms in eq. 1.4. Now we need to choose the specific kernel K and with it H . As mentioned above, the sub-Ohmic behaviour follows for the kernel $K(t) = K_0 t^{-\alpha} \rightarrow K(s) = K_0 \frac{\Gamma(-\alpha+1)}{s^{-\alpha+1}}$.

$$\begin{aligned}
\langle X^2(s) \rangle &= \mathcal{L} \left(2k_b T \int_0^t H(t') dt' \right) \\
&= 2k_b T \frac{1}{s} H(s) \\
&= 2k_b T \frac{1}{Ms^3 + K_0 \Gamma(1-\alpha) s^{\alpha-1}} \tag{1.5}
\end{aligned}$$

Since we are mainly interested in the long term behaviour of $\langle X^2(t) \rangle$ we need only look at the $s \rightarrow 0$ asymptotics.

$$\begin{aligned}
\langle X^2(s) \rangle &\sim 2k_b T \frac{s^{-\alpha-1}}{K_0 \Gamma(1-\alpha)} \\
\langle X^2(t) \rangle &\sim 2k_b T \frac{t^\alpha}{K_0 \Gamma(1-\alpha) \Gamma(\alpha)} \\
&= 2k_b T \frac{\sin \pi \alpha}{K_0 \pi} t^\alpha
\end{aligned}$$

Note that $\alpha = 1$ is not represented in this case, since for the ohmic bath case the Laplace transform would have read $K(s) = K_0$. Recalculating the relevant steps this leads to

$$\begin{aligned}\langle X^2(t) \rangle &= 2k_b T \frac{1}{K_0} t \quad , \alpha = 1 \\ &= 2k_b T \frac{\sin \pi \alpha}{K_0 \pi} t^\alpha \quad , 0 < \alpha \leq 1\end{aligned}$$

This gives us the relevant diffusion coefficients of the model.

Equation 1.5 also allows us to identify the ballistic behaviour time scale of the GLE. We note that for s arbitrarily large, the s^1 dominates the $s^{\alpha-1}$ dependence in the denominator of $H(s)$ eventually

$$\begin{aligned}Ms &\gg K_0 \Gamma(1-\alpha) s^{\alpha-1} \\ \frac{M}{K_0 \Gamma(\alpha-1)} s^{2-\alpha} &\gg 1 \\ s^{2-\alpha} &\gg \frac{K_0 \Gamma(1-\alpha)}{M} \\ s &\gg \left(\frac{K_0 \Gamma(1-\alpha)}{M} \right)^{\frac{1}{2-\alpha}}\end{aligned}$$

Since s has the dimension of inverse time, we can expect behaviour $\langle X^2(s) \rangle \sim 2k_b T \frac{1}{Ms^3}$ or $\langle X^2(t) \rangle \sim 2k_b T \left(\frac{t^2}{M} \right)$ on scales smaller than $t_b = \left(\frac{M}{K_0 \Gamma(1-\alpha)} \right)^{\frac{1}{2-\alpha}}$. In the case of $\alpha = 1$, there is again a discontinuity in the kernel to look out for and instead the calculation reads

$$\begin{aligned}Ms &\gg K_0 \\ s &\gg \frac{K}{M}\end{aligned}$$

or $t_b = \frac{M}{K_0}$, our already known relation for the ballistic time scale of the Langevin equation.

1.5 SETTING THE BATH PARAMETERS

The bath is determined by setting the masses m_j , the frequencies ω_j and the coupling constants k_j , this all for a not yet determined bath size N . This is a staggering amount of free parameters and while some trial and error cannot be avoided, a few good guesses can be made. The most important parameter to determine is the bath size, since it corresponds directly to the computational effort needed for integration. The main thrust of the argument here will be that the bath essentially serves as a sum approximation to the kernel and random force and hence these are the starting point for determining the bath size.

For sufficiently dense frequencies, we approximate the kernel via 1.3 so

$$\begin{aligned} K(t) &= \sum_j k_j \kappa_j^2 \cos \omega_j t \\ &\approx \int_0^\infty g(\omega) k(\omega) \kappa^2(\omega) \cos \omega t d\omega \end{aligned}$$

Since our kernels are of the form $K(t) = K_0 t^\alpha$ and the integral is essentially an inverse fourier transform, it follows then from any table of transforms [1]. In the mobile bath case $\kappa^2 = 1$, so that

$$g(\omega) m(\omega) \omega^2 = \frac{2}{\sqrt{2\pi}} K_0 \Gamma(1-\alpha) \sin\left(\frac{\pi\alpha}{2}\right) \omega_j^{\alpha-1}$$

If we for the moment assume all bath masses to be equal $m(\omega) = m_b$, the density distribution $g(\omega)$ becomes non uniform and we can use it to estimate the number of bath oscillators in the relevant frequency band needed. We want to simulate the system on step sizes smaller than ballistic time scale of the resulting GLE behaviour, so on time scales smaller than the ballistic time scale $\omega_{\max} = \frac{1}{t_b}$. The lowest frequency of concern should scale inverse to the simulation length t_E , so that $\omega_{\min} = \frac{1}{t_E}$. Then we have:

$$\begin{aligned} N &= \int_{\omega_{\min}}^{\omega_{\max}} g(\omega) d\omega \\ &= \int_{\omega_{\min}}^{\omega_{\max}} \frac{1}{m_b} \frac{K_0}{\Gamma(\alpha) \cos \frac{\pi\alpha}{2}} \omega^{\alpha-3} d\omega \\ &\sim \frac{1}{(\alpha-2)m_b} \frac{K_0}{\Gamma(\alpha) \cos \frac{\pi\alpha}{2}} \omega_{\min}^{\alpha-2} \quad (\omega_{\min} \rightarrow 0) \end{aligned}$$

On the other hand we have the relation

$$\begin{aligned} t_b &= \left(\frac{M}{K_0 \Gamma(1-\alpha)} \right)^{\frac{1}{2-\alpha}} \\ t_b^{2-\alpha} &= \frac{M}{K_0 \Gamma(1-\alpha)} \\ \omega_{\max}^{-2+\alpha} &= \frac{M}{K_0 \Gamma(1-\alpha)} \\ K_0 &= \frac{M}{K_0 \Gamma(1-\alpha)} \omega_{\max}^{-2+\alpha} \end{aligned}$$

So that we get

$$\begin{aligned} N &\sim \left(\frac{1}{(\alpha-2)m_b} \frac{1}{\Gamma(\alpha) \cos \frac{\pi\alpha}{2}} \omega_{\min}^{\alpha-2} \right) \left(\frac{M}{K_0 \Gamma(1-\alpha)} \omega_{\max}^{-2+\alpha} \right) \\ &\propto \frac{M}{m_b} \left(\frac{\omega_{\min}}{\omega_{\max}} \right)^{\alpha-2} \\ &= \frac{M}{m_b} \left(\frac{t_E}{t_b} \right)^{2-\alpha} \end{aligned}$$

From this we can read these important properties of the simulation complexity needed:

- The scaling punishes heavier distinguished particles in direct proportion to their relative mass compared to the bath masses.
- the scaling is worse than proportional to the simulation length and gets worse the lower α is chosen. If we want to simulate three orders of magnitude compared to the ballistic time scale, very close to $\alpha = 1$ only ca. 1000 bath oscillators are needed (setting $\frac{M}{m_b} = 1$) but for α close to zero a truly enormous bath of 10^6 oscillators is needed.
- Since the required number of calculations is in itself also proportional to the bath size and length of the simulation, that means in the we are doubly penalized for longer simulation lengths and low α values become prohibitive

Again taking into account the discontinuity at $\alpha = 1$ we have to use $\omega_{\max} = \frac{K_0}{M}$ and $N = \int_{\omega_{\min}}^{\omega_{\max}} \frac{K_0}{m_b} \omega^{-2} d\omega$. Repeating the steps above yields

$$N \propto \frac{M}{m_b} \left(\frac{t_E}{t_b} \right)^1$$

So the scaling of the $\alpha < 1$ calculation is preserved (but without the divergency in the Gamma function).

In this work we will be using a uniform frequency distribution instead for ease of simulation, so there is no strict guarantee that the above scaling is reproduced in our bath and we need to check explicitly for appropriate bath sizes. Never the less these derivations give us pointers for the bath sizes and limitations of these simulations.

The scaling of the bath oscillators needed can be somewhat improved at least by changing the coupling constants slightly. The idea here is to choose these constants in way that the sum approximation of the kernel

$$K(t) \approx \sum_{j=1}^N k_j \kappa_j^2 \cos \omega_j t$$

converges faster than the rectangle rule considered up until this point. We choose the Simpson rule of integration, which simply rescales the k_j according to.

$$k_j \Leftarrow \begin{cases} \frac{1}{3}k_j & j = 0, j = N \\ \frac{2}{3}k_j & j \text{ odd} \\ \frac{4}{3}k_j & j \text{ even} \end{cases}$$

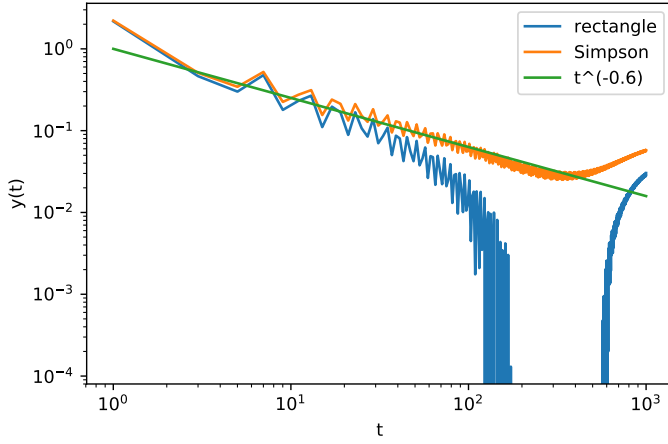


Figure 1.1: Comparison log-log plot of kernel approximation between rectangle and Simpson scheme. 1000 terms are used in the sum approximation of the kernel $K(t) = t^{-0.6}$.

| | ohmic bath | sub-ohmic bath |
|------------------------------|---|--|
| D | $\frac{k_b T}{K_0}$ | $k_b T \frac{\sin \pi \alpha}{K_0 \pi}$ |
| k_j (before Simpson shift) | $\frac{2}{\sqrt{2\pi}} K_0 \Delta \omega$ | $\frac{2}{\sqrt{2\pi}} K_0 \Gamma(1 - \alpha) \sin\left(\frac{\pi \alpha}{2}\right) \omega_j^{\alpha-1} \Delta \omega$ |
| ballistic time t_b | $\frac{K_0}{M}$ | $\left(\frac{M}{K_0 \Gamma(1 - \alpha)}\right)^{\frac{1}{2-\alpha}}$ |

Table 1.1: Important bath parameters and values for the fully mobile bath, $\kappa = 1$ with uniform frequency distribution of spacing $\Delta \omega$.

For n points equally spaced in the integration interval (a, b) the rectangle rule has an error scaling with $\propto \frac{(b-a)^2}{n}$ compared to the Simpson rules $\propto \frac{(b-a)^5}{n^4}$. For the kernel considered in the sub-ohmic case with a mobile bath and a uniform frequency distribution (so that $k_j = \frac{2}{\sqrt{2\pi}} K_0 \Gamma(1 - \alpha) \sin\left(\frac{\pi \alpha}{2}\right) \omega_j^{\alpha-1} \Delta \omega$) we can plot the behaviour with and without the Simpson's rule shift. Fig 1.1 shows both the rectangle and Simpson approximation to the kernel $K(t) = t^{-0.6}$ in the interval $[1.0, 1000.0]$ with 1000 terms in the sum and $\omega_{\max} = 2.0$, $\omega_{\min} = 5 \cdot 10^{-5}$. As we can see, even for this comparatively low number of terms the Simpson approximation produces the right scaling behaviour over at least half the shown time scale, a considerable improvement over the rectangle scheme which doesn't even reach a tenth of the timescale before breaking off from the desired $t^{-0.6}$ scaling behaviour.

Because of the amount of parameters and the case separation between ohmic and sub-ohmic behaviour, table 1.1 gives a brief overview of the most important ones.

Part II
IMPLEMENTATION

2

THE ALGORITHM

In this chapter we will present the simulation method applied and an overview of problems and limitations on the simulation as well as some tests on accuracy and convergence of the model.

2.1 THE VELOCITY VERLET METHOD

A well known integrator for linear differential equations used in molecular dynamics simulation is the Verlet method[15]. This method utilizes time symmetric integration steps to ensure that our error in the total energy is globally bounded $\propto h^2$ with integration step length h . This is essential for our heat bath simulation, since we demand a well defined equilibrium temperature and hence total bath Energy for the system to model our GLE.

There are several variants of the algorithm, the one used here will be the following using two half steps. For a step size h and potential ϕ as well as coordinate q :

$$\begin{aligned} p &= p_n - \frac{h}{2} \phi'(q_n) \\ q_{n+1} &= q_n + hp \\ p_{n+1} &= p - \frac{h}{2} \phi'(q_{n+1}) \end{aligned}$$

Since all our potentials are essentially harmonic, we will look at the energy error in a timestep of a hamiltonian of the form $H = \frac{q^2}{2} + \frac{p^2}{2}$ (setting masses and constants to one for simplicity)

$$\begin{aligned}
\Delta H &= H(v_0, q_0) - H(p_1, q_1) \\
&= \frac{p_0^2}{2} + \frac{q_0^2}{2} - \frac{1}{2} \left(p - \frac{h}{2} \phi'(q_1) \right)^2 - \frac{1}{2} (q_0 + hp)^2 \\
&= \frac{p_0^2 + q_0^2}{2} - \frac{1}{2} \left(p_0 - \frac{h}{2} \phi'(q_0) - \frac{h}{2} \phi'(q_1) \right)^2 - \frac{1}{2} \left(q_0 + h \left(p_0 - \frac{h}{2} \phi'(q_0) \right) \right)^2 \\
&= \frac{p_0^2 + q_0^2}{2} - \frac{1}{2} \left(p_0 - \frac{h}{2} (q_0 + q_1) \right)^2 - \frac{1}{2} \left(q_0 + h \left(p_0 - \frac{h}{2} q_0 \right) \right)^2 \\
&= \frac{p_0^2 + q_0^2}{2} - \frac{p_0^2}{2} + \frac{p_0 h}{2} (q_0 + q_1) - \frac{h^2}{8} (q_0 + q_1)^2 \\
&\quad - \frac{q_0^2}{2} - h q_0 \left(p_0 - \frac{h}{2} q_0 \right) - \frac{h^2}{2} \left(p_0 - \frac{h}{2} q_0 \right)^2 \\
&= \frac{p_0 h}{2} (q_0 + q_1) - \frac{h^2}{8} (q_0 + q_1)^2 - h q_0 \left(p_0 - \frac{h}{2} q_0 \right) - \frac{h^2}{2} \left(p_0 - \frac{h}{2} q_0 \right)^2 \\
q_0 + q_1 &= q_0 + q_0 + hp = 2q_0 + h \left(p_0 - \frac{h}{2} q_0 \right) \\
&= 2q_0 + h(p_0 - hq_0) \\
\Delta H &= \frac{p_0 h}{2} (2q_0 + hp_0) - \frac{h^2}{8} (2q_0)^2 - h q_0 \left(p_0 - \frac{h}{2} q_0 \right) - \frac{h^2}{2} (p_0)^2 + O(h^3) \\
&= p_0 q_0 h + \frac{p_0^2}{2} h^2 - \frac{q_0^2}{2} h^2 - q_0 p_0 h + \frac{q_0^2}{2} h^2 - \frac{h^2}{2} p_0^2 + O(h^3) \\
&= 0 + O(h^3)
\end{aligned}$$

So the error is indeed of third order in the step size. Since $N = \frac{t_E}{h}$ such steps are necessary up until time t_E the global error in energy scales $O(h^2)$. This allows us to define a bath temperature T and expect it to remain reasonably constant over the whole run.

2.1.1 Impulsive Verlet

Now the multiple implementation schemes for Velocity Verlet are equivalent only for velocity independent system potentials. Since our hard boundaries induces rapid velocity changes upon reflection, not only do these different schemes produce different results upon boundary contact, the change upon reflection is explicitly dependent on the velocity direction on contact. The global error bound from the algorithm is lost, trial and error has shown that depending on the scheme used the system either heats up or cools down with each boundary contact in our simulations.

Luckily, the problem of Verlet type integrations with hard boundaries has been studied, the modified algorithm that is the result of these studies being called Impulsive Verlet[5]. We will give an overview of the solution found here. Y A. Hounoungbo and B. B. Laird have shown that in a one dimensional system with a hard boundary at

Algorithm 2.1 Impulsive Verlet step of size h

```

1:  $t_{\text{remain}} \leftarrow h$ 
2: while  $t_{\text{remain}} > 0$  do
3:   find first contact time  $t_c$  with targets, if any, else  $t_c \leftarrow t_{\text{remain}}$ 
4:   do Velocity Verlet step of size  $t_c$ 
5:   reflect  $p$ 
6:    $t_{\text{remain}} \leftarrow t_{\text{remain}} - t_c$ 
7: end while

```

point δ that on each collision within a timestep a jump in Energy of the form

$$\Delta H = -\phi'(\delta) (h_b - h_{\sharp}) p$$

is introduced, $h_{\sharp} = h - h_c$ and $h_b = h - h_{\sharp}$ the parts of the jump step happening before and after the contact at h_c . This means that an error of $O(h)$ is introduced globally on the Energy if contacts happen regularly except in three cases:

1. the external potential vanishes on contact
2. $(h_b - h_{\sharp}) = 0$, the contact happens exactly in the middle of the step
3. no contacts happen within timesteps.

The authors settled on the third case for implementations and have then shown via testing that the global energy bound is restored in this way. The resulting algorithm was dubbed the 'Impulsive Verlet' method, see algorithm 2.1, and will be the method used in this work.

Depending on the boundary and dimension of the problem, finding the collision time in the time step can be somewhat difficult, for example for the case of contact with a sphere of radius R at point t it involves finding the roots of a quartic polynomial:

$$\begin{aligned} 0 &= \|q(h_c) - t\|^2 - R^2 \\ &= \|q_n + h_c p_{n+1/2}\|^2 - R^2 \\ &= \left\| q_n + h_c \left(p_n - \frac{h_c}{2} \phi'(q_n) \right) \right\|^2 - R^2 \end{aligned}$$

This means in practice that depending on the geometry we have to check for errors in the root finding method and for boundary penetration.

2.2 TESTING THE MODEL

With the Integration method specified, the whole algorithm we used reads in pseudo code form as algorithm 2.2

Algorithm 2.2 heat bath simulation

```

1: generate frequencies uniformly in  $\left[ \frac{1}{2 \cdot t_{\text{END}}}, 5 \cdot \frac{1}{t_{\text{ballistic}}} \right]$ 
2: set masses and coupling constants for the bath according to  $\alpha$  for
   the mobile bath
3: shift masses and coupling constants to satisfy Simpson rule
4: for  $i \leq \# \text{Simulations}$  do
5:   draw intial values from bath from Boltzmann distribution
6:   set initial values to zero for distinguished particle
7:   set integration step size  $\frac{1}{10 \cdot t_{\text{ballistic}}}$ 
8:   while  $t < t_{\text{END}}$  do
9:     Impulsive Verlet Step
10:    end while
11:    update measured mean values (MSD, kinetic Energy, etc.)
12: end for

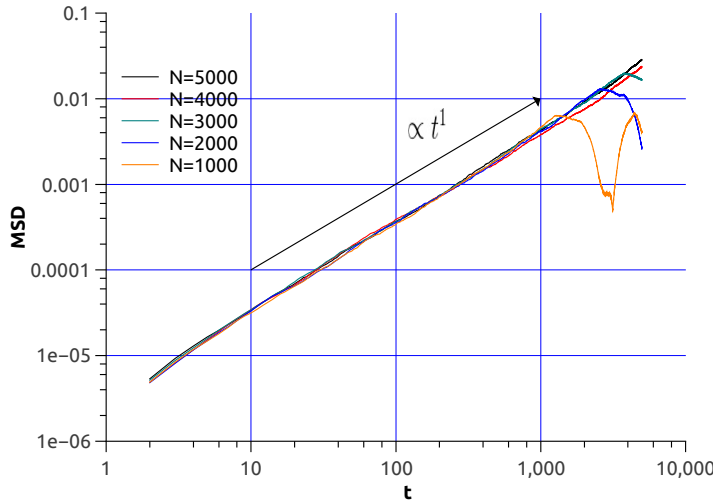
```

First we shall demonstrate that the free and generalized Langevin behaviour can be modeled with the bath and the Verlet integration method and we will test for the bath sizes needed for the integration lengths and parameters used in the geometries of the next chapter.

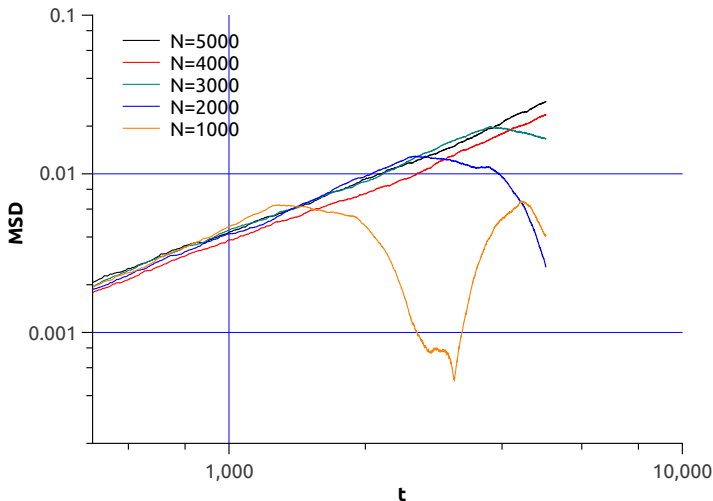
In a second step we will show that the Impulsive Verlet method works in the sense that the global energy bound is of the order of the original Verlet method and thus the bath temperature is sharply defined for the simulations.

2.2.1 The free behaviour

At first we will have a look at the ohmic case. As mentioned in the first chapter, all simulations will be done at $T = 100\text{K}$ with a distinguished particle of mass set to one, $m = 1\text{g}$. The longest simulation times in our reflecting systems will be up till 5000s , so we will first test for the bath size needed to get the regular Langevin MSD behaviour proportional to t . We expect this number to scale directly with the 5000s , from our observations towards the scaling behaviour of the bath. The most obvious measure of quality of our simulations is the correctness of the scaling behaviour of the MSD over the whole time scale, so figure 2.1 shows the measured MSD for different numbers of oscillators. The plots are double logarithmic, so that according to $\log(y) = \log(Ax^\alpha) = \log(A) + \alpha \cdot \log(x)$ the scaling behavior can be easily read off the slope of $\log(y)$ as a function of $\log(x)$.



(a) log-log plot of MSD. The arrow indicates a line of slope one for easier comparison

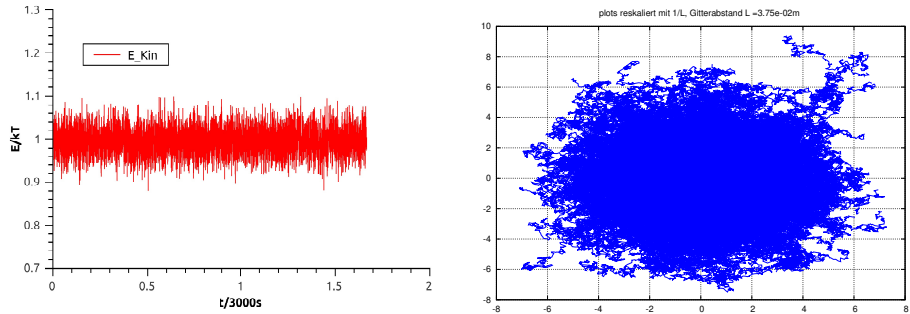


(b) same plot zoomed in at end time

Figure 2.1: MSD for different bath sizes in the $\alpha = 1$ case and two dimensions . Averages taken over 1000 simulations.

As we can see, 4000 oscillators suffice to produce the correct slope $\alpha = 1$ over the full simulation length. In the case of insufficient bath sizes, the MSD shows at first a horizontal behaviour, which makes spotting the mistake in the MSD easy by eye. Next we need to make sure the kinetic Energy is appropriately defining a constant temperature over the full length of the simulation, else the notion of a heat bath becomes absurd. Also depicted in figure 2.2 are example plots of the distinguished particle.

Figure 2.2: Results for the free integration case for $\alpha = 1$. $N = 5000$ bath particles used and simulated in 2 dimensions.



(a) Kinetic energy of the distinguished particle rescaled by $k_b T$. Values are the averages over 1000 simulations.

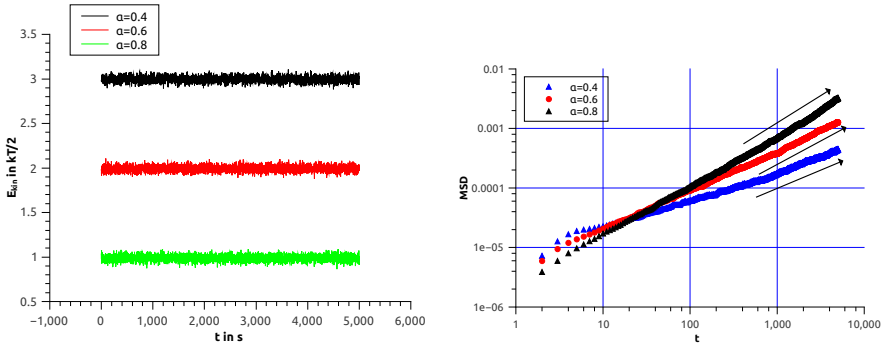
(b) 500 example plots of x and y coordinates of the distinguished particle, rescaled by length $L = 3.75 \cdot 10^{-2}$ m. (the algorithm is lattice based for later tests, so it needs a lattice scale for reference even in an empty lattice)

The kinetic Energy of the distinguished particle is sharply defined around its' equilibrium value $\langle v^2 \rangle = 2 \frac{k_b T}{m}$, as they should be. We can read off the relative standard deviation of the temperature from the kinetic Energy plot to be $\approx 5\%$, which according to the Einstein relation $D = \mu k_b T$ we can interpret as the uncertainty ΔD when measuring the diffusion coefficient in reflecting systems.

THE SUB-OHMIC CASE

Next we need to reproduce these checks in the case of $\alpha < 1$. For consistency, henceforth all subohmic measurements will be done at the values $\alpha = 0.4$, $\alpha = 0.6$, and $\alpha = 0.8$. Firstly we observe the scaling depending on the bath sizes. Instead of repeating the MSD comparisons for a full range of different bath sizes, for the sake of brevity, we will settle at first for a maximum computational effort we are willing to spend of $N = 14k$ for initial tests and look if these values of α are correctly reproduced. Again, from our considerations in chapter one, we expect the bath behaviour to get worse the lower we pick α .

Figure 2.3: Results for the free integration case for $\alpha < 1$. All Plots are averages over 1000 simulations at $T = 100K$.



(a) Kinetic energy of distinguished particle as function of time rescaled by thermal equilibrium energy $\frac{k_B T}{2}$. Plot for $\alpha = 0.6$ and $\alpha = 0.4$ shifted upward by one respectively two for easier visibility.

(b) log-log Plots of MSD versus time. The arrows indicate the expected slopes 0.8, 0.6 and 0.4 for easier comparison by eye.

As we can see from figure 2.3 in all three cases we achieve equally sharply defined bath temperatures over the whole run. The $\alpha = 0.8$ plot exhibits the correct scaling of the MSD over almost the full time regime aside from the initial ballistic behaviour until equilibration. As expected the other two plots corresponding to the lower α values show a slower transition from ballistic to diffusive regime. We can also see that while the MSD for the lower two values approaches the right slope asymptotically, the arrows indicating the correct behaviour are not fully parallel to the plots, through trial and error we found the bath sizes to be working appropriately in figure 2.4.

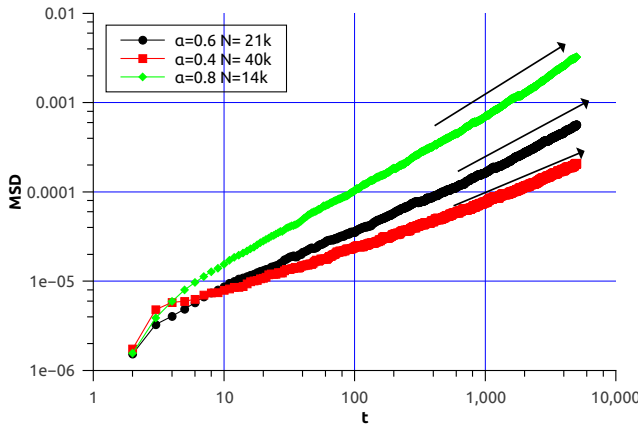


Figure 2.4: log-log plots of MSD versus time. The arrows indicate the expected slopes 0.8, 0.6 and 0.4 for easier comparison by eye. The bath sizes are 14k, 21k and 40k.

2.3 TESTING THE REFLECTING CASE

The last question to be answered is whether or not our implementation of the impulsive Verlet method preserves the energy error and hence bath temperature as it should. We will use the geometries simulated in the next chapter for these checks, that is a lattice of spherical obstacles in two dimensions and the one dimensional box with hard walls. Each test will be done once for normal and once for subdiffusion.

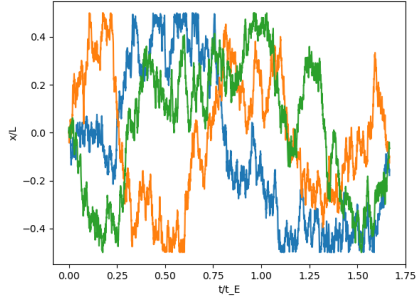
For the particle trapped in an interval with reflecting boundaries we expect the energy error to behave exactly as in the free case. This is due to the energy error induced by reflection. It is essentially of the order of the difference between numerically approximated and actual time of reflection. For the sphere we have to search for the roots of a quartic equation and hence have a finite accuracy (and always run the risk of missing roots). For the reflecting wall the time of reflection can be evaluated analytically. Let the wall be at point $X = \delta$ and the contact happen at the first step for simplicity. Then:

$$\begin{aligned}\delta &= q(h_c) \\ &= q_0 + h_c v_{1/2} \\ &= q_0 + h_c (v_0 + h_c v_0)\end{aligned}$$

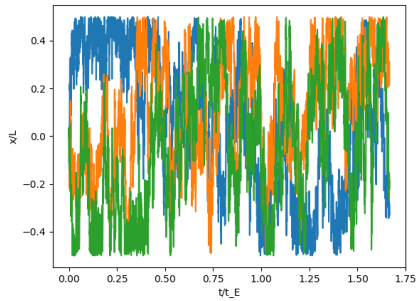
So at each step we only have to search whether or not the known roots of the polynomial of degree two lie within the time step. For the 2-d spheres, there is always the risk of overlooking roots (essentially missing short glancing contacts).

2.3.1 Testing on a 1-d box

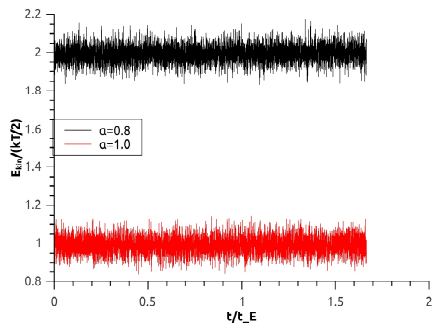
The geometry will be set up so that the distinguished particle starts in the middle of a box of size L with reflecting walls at $\pm \frac{L}{2}$. The size of the box will be chosen such that the averaged MSD of the particle covers the whole interval in $t_E = 800s$ (for the infinite bath size coefficient of diffusion, see table 1.1). The choice of t_E is of course arbitrary for testing as long as it is small compared to the simulation time, so we are not oversampling the regime of free particle diffusion. The test is done once for the ohmic bath and once for $\alpha = 0.8$.



(a) three example trajectories for the ohmic case in a box of lenght L



(b) three example trajectories for the sub-ohmic case in a box of lenght L



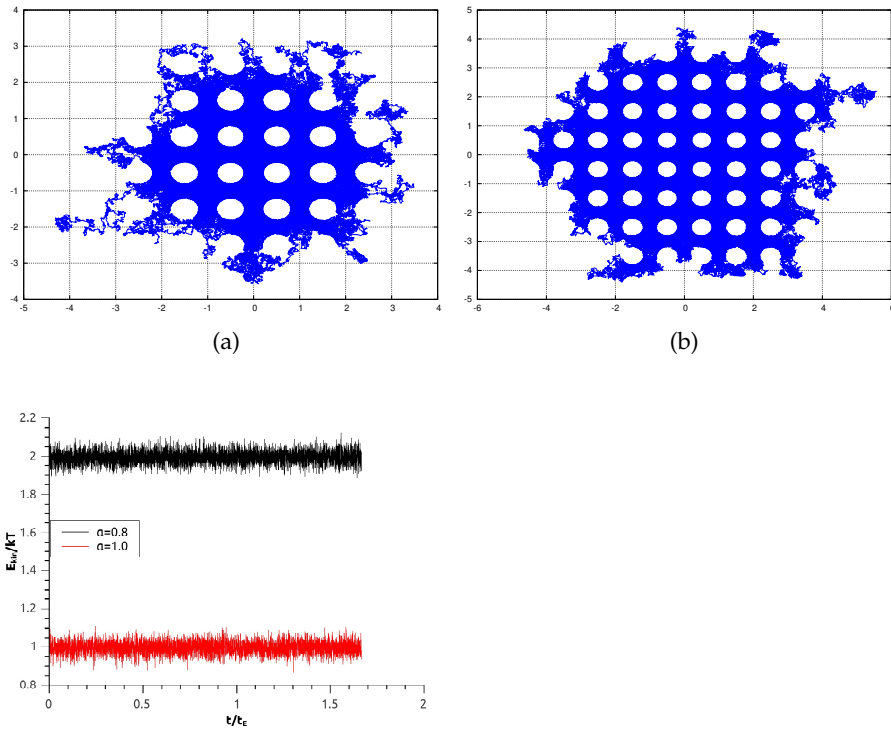
(c) plot of the kinetic energy of the distinguished particle as a function of time. The energies are rescaled by the equilibrium kinetic energy $k_b \frac{T}{2}$. The plot for the subohmic behaviour is shifted upwards by one for readability

Figure 2.5: Results for the box with reflecting boundaries. All plots are averages over 1000 simulations at $T = 100K$. Times are rescaled by $t_E = 800s$ and lengths by $L = \sqrt{2D_\alpha t_E^\alpha}$ for easier reading. Figure 2.5a shows three example plots of the particle position as a function of time for the ohmic case, figure 2.5b for the $\alpha = 0.8$ case. The bath size is $N = 14k$.

As we can see from figure 2.5c the kinetic energy is still sharply defined as should be, though fluctuations around the equilibrium can be roughly read off to be 5% as expected.

2.3.2 Testing on a 2-d lattice of spheres

The case of periodically ordered spheres as scatterers is sometimes called the periodic Lorentz gas in the diffusion literature[8, 10, 11] and will be the second system of interest here. The system consists of a quadratic lattice of constant size L , the particle again is starting in the center of a lattice cell, the spheres are located at the cell corners. The size of the lattice will be chosen such that the averaged MSD of the particle covers a whole cell at $t_E = 800s$. The test is done once for the ohmic bath and once for $\alpha = 0.8$. In contrast to the box case we also have a second length to specify here, namely the sphere radii. These are chosen in a way so that the cell consists to $\phi = 30\%$ of reflecting obstacles. ϕ and the radius r are related by $\frac{\pi r^2}{L^2} = \phi$.



(c) plot of the kinetic energy of the distinguished particle as a function of time. The energies are rescaled by the equilibrium kinetic energy $k_b T$. The plot for the subohmic behaviour is shifted upwards by one for readability

Figure 2.6: Results for the box with reflecting boundaries. Energy plots are averages over 1000 simulations at $T = 100K$. Times will be rescaled by $t_E = 800s$ and lengths by $L = \sqrt{2D_\alpha t_E^\alpha}$ for easier reading. D_α is the expected diffusion coefficient for the infinite bath as derived in chapter one. Figure 2.6a shows 500 example plots of the particle x - position as a function of the particle y - position for the ohmic case, figure 2.6b for the $\alpha = 0.8$ case.

Again, the original relative energy error of $\approx 5\%$ is achieved in figure 2.6c.

2.3.3 summing it up

We have demonstrated that our implementation of the impulsive Verlet method preserves the prime measure of the quality of our heat bath, compared to the original Verlet algorithm over the full time range used in subsequent results for both reflecting systems of interest. We have also shown that for the computational effort we settled on, the MSD of the distinguished particle shows the expected behaviour for the ohmic and $\alpha = 0.8$ case over the full simulation time. As expected the behaviour of the model gets worse in simulation for

smaller values of α , though the systems still behaves subdiffusive for long times, though the scaling behaviour seems to be slightly off.

3

SIMULATION RESULTS

This chapter will first compare results for simulations of the ohmic case with some known results and then focus on the case of subdiffusive Diffusion. In the case of an ohmic heat bath we can also compare our results versus a standard numerical implementation of the Langevin Equation. The scheme will be a discretization of the equations in the time step of size Δ as follows

$$\begin{aligned} m(v(t + \Delta) - v(t)) &= -\gamma \int_t^{t+\Delta} v(s) ds + \int_t^{t+\Delta} F_R ds \\ &\approx \gamma v(t) \Delta + A \cdot n_{01} \\ x(t + \Delta) - x(t) &\approx v(t) \Delta \end{aligned}$$

Here we assume the integral over the stochastic force behaves like a normally distributed random variable n_{01} (independent for each step) times a yet to be determined factor. Using the fluctuation-dissipation relation we get

$$\begin{aligned} \left\langle \int_{t_1}^{t_1+\Delta} F_R ds \int_{t_2}^{t_2+\Delta} F_R ds \right\rangle &= A^2 \cdot \langle n_{01} n'_{01} \rangle \\ &= \int_{t_1}^{t_1+\Delta} \int_{t_2}^{t_2+\Delta} \underbrace{\langle F_R(s') F_R(s) \rangle}_{k_B T \delta(s-s')} ds ds' \\ &= \begin{cases} k_B T \Delta & \text{if the intervals of integration overlap} \\ 0 & \text{else} \end{cases} \\ \hookrightarrow \|A\| &= \sqrt{k_B T \Delta} \end{aligned}$$

To allow better comparison with our model we will also search for the time of first contact with reflecting object in each step and integrate only till that time, so that as in the impulsive Verlet schemes contacts do not happen within steps. The Verlet integrations are all done for $K_0 = 1$, $T = 100K$ until $t_{end} = 5000s$ for integration steps dependent on the ballistic time scale $\Delta t = \frac{t_b}{10}$. The distinguished particle of mass $M = 1g$ is initialized in a thermalized state at position 0.

3.1 SIMULATION IN A 2-D LATTICE OF SPHERES

We will explore the behaviour of the system in a lattice of reflecting spheres, the periodic Lorentz gas[10]. Two questions are of interest

here: do the spheres change the nature of the scaling (i.e is the resulting (sub)diffusion scaling with a different α') and how does the diffusion coefficient change in the presence of spheres.

The geometry is as in the tests, that is the particle starts in a square lattice of spheres at the corners of each lattice cell, with lattice size L . It is convenient to determine the spheres of radii r via the concentration ϕ of the spheres in the lattice

$$\phi = \frac{\pi r^2}{L^2}$$

Obviously ϕ has a maximum values when the spheres are in contact, $\phi \leq \phi_c = \frac{\pi(\frac{L}{2})^2}{L^2} = \frac{\pi}{4}$. We start again with the ohmic case before we consider the sub-ohmic bath.

3.1.1 Results in the ohmic case

For the ohmic case there are of known results for our geometry which we will briefly sum up here. Firstly, there are solutions known for the conductivity of fully insulating spheres ($\sigma_{\text{sphere}} = 0$) in a square lattice, embedded in a matrix of conductiviy σ . These results can be applied to our case, because of the similiarites of the Focker-Planck [14] equation to the governing equations of electrostatics, though the Langevin behaviour and the Fokker Planck behaviour need not necessarily be the same on all time and length scales. Still, this gives us a baseline of comparison. The result is found in a recursive manner, the third order approximation is [12]:

$$\frac{D(\phi)}{D(0)} = 1 - 2\phi \left(1 + \phi - \frac{0.305\phi^4}{1 - 1.404\phi^8} - 0.013\phi^8 \right) \quad (3.1)$$

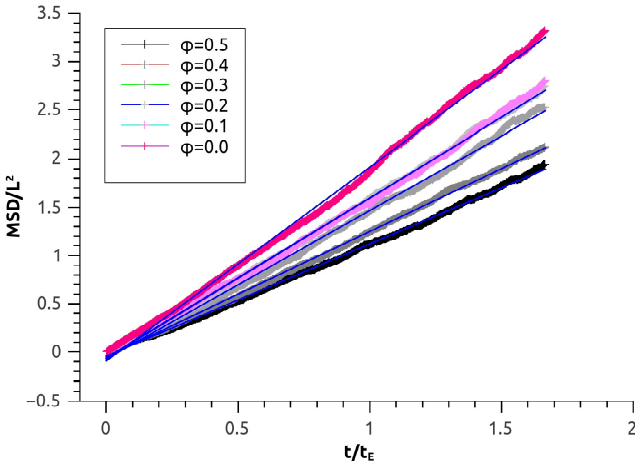
Given these considerations we settle on $t_E = 3000s$ and the corresponding lattice constant L . The most dillute sytem we will simulate will be at $\phi = 0.1$, which then gives us a sphere radius of

$$r_{0.1} = L \frac{\sqrt{0.1}}{\pi} \approx 0.1 \cdot L$$

So we have to ensure that the system is actually diffusive on the Length scale of these spheres. Let l_b be the length scale associated with the ballistic time scale, $l_b = \sqrt{\langle v^2 \rangle_{\text{eq}} t_b^2}$. Then we have to check:

$$\begin{aligned} l_b &< 0.1 \cdot L \\ \frac{K_0}{\sqrt{M}} \sqrt{k_b T} &< 0.1 \cdot \sqrt{\frac{4D}{t_E}} \\ \frac{K_0}{\sqrt{M}} \sqrt{k_b T} &< 0.1 \cdot \sqrt{\frac{4 \frac{k_b T}{K_0}}{t_E}} \\ \frac{K_0}{M^{3/2}} &< 0.2 \cdot \sqrt{\frac{1}{K_0 t_E}} \end{aligned}$$

Figure 3.1: MSD for different sphere concentrations ϕ together with linear fits. All simulations for 14k bath particles at 100K temperature. All times have been rescaled by the lattice scale time $t_E = 3000s$, all MSD by the squares lattice constant L^2 .



Plugging in the chosen values $M = 1g, K_0 = 1\frac{g}{s}$ and dividing by the leftover dimension on $g^{-1/2}$

$$1 < 0.2 \cdot \sqrt{\frac{1}{3000}} \approx 0.004$$

So our chosen parameters ensure we are in the appropriate regime, enough so that we can reuse them later for the subohmic baths when the ballistic time scale increases the lower α is picked. We will simulate the lattice for values in the range $\phi \in [0.1, \dots, 0.5]$, noting here that higher values of ϕ increasingly slow down the simulation as the stepsize of the impulsive Verlet method decreases on average close to reflecting boundaries and on the other hand small spheres may be overlooked by our collision detection if the time inside the sphere is shorter than the subintervalls of the steps we test on .

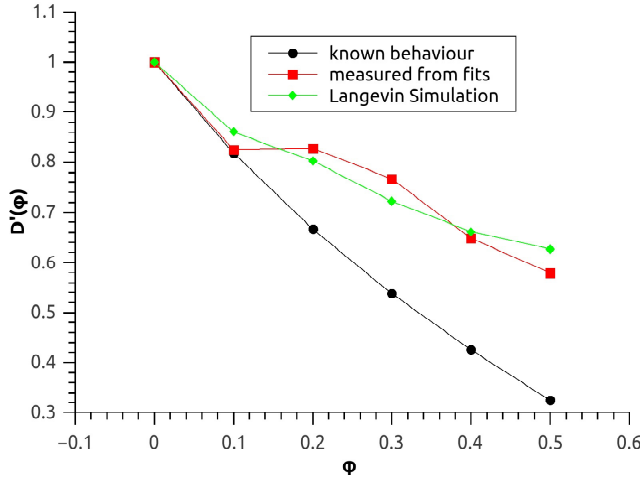
We plot the resulting MSD graphs in figure 3.1, together with linear fits. We can immediately see two things then: the nature of the diffusion does not change with the concentration of the spheres in the sense that all graphs show normal diffusion. Secondly the coefficient of diffusion, the slope in the graphs, decreases with increasing ϕ , as one would expect.

We can get the individual diffusion coefficients from the linear fits. For better comparison with the known results, we rescale them by the measured free diffusion coefficient

$$D'(\phi) = \frac{D_{\text{fit}}(\phi)}{D_{\text{fit}}(0)}$$

Plotting the result together with the previously discussed curves and the langevin simulation in the same geometry then gives us.

Figure 3.2: plot of relative coefficients of diffusion $D'(\phi) = \frac{D(\phi)}{D(0)}$ as functions of volume fraction ϕ , from our fits of the heat bath simulation and the Langevin simulation, as well as according to equation 3.1



As we can see, our measured behaviour deviates for $\phi > 0.1$, at which point the model has higher effective diffusion coefficients than expected. Stated another way, for higher concentrations the model behaves as if the spheres were smaller than actually implemented. This behaviour is consistent with the results of the Langevin implementation, pointing towards the discrepancy being a result of the parameter choices of the simulation rather than the implementation scheme itself.

3.1.2 Results in the subohmic case

All considerations are as above (adjusted for the different alpha). The only difference being that we will use fits involving power laws now and that to our knowledge there are no known results for the subdiffusive Langevin Equation in this geometry to compare to. The fits:

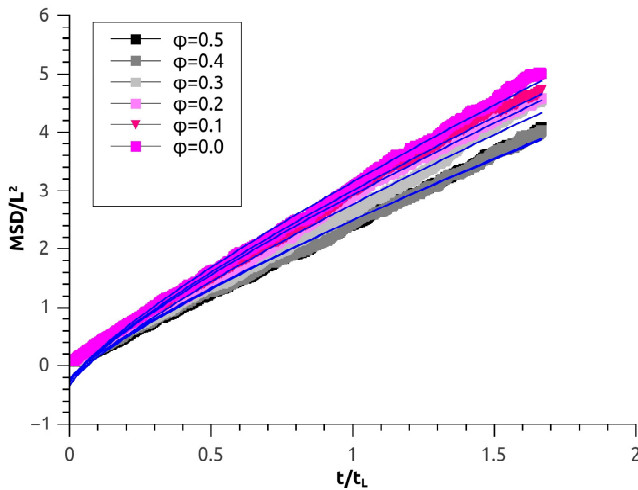
$$y_{\text{fit}, \alpha}(t) = A + D_{\text{fit}} \cdot t^\alpha$$

yield figure 3.4a. We can see that for the $\alpha = 0.4$ plot the diffusion coefficient actually increases, which is probably a good indicator that even 40k bath particles are too few to properly implement this bath rather than an actual physical effect.

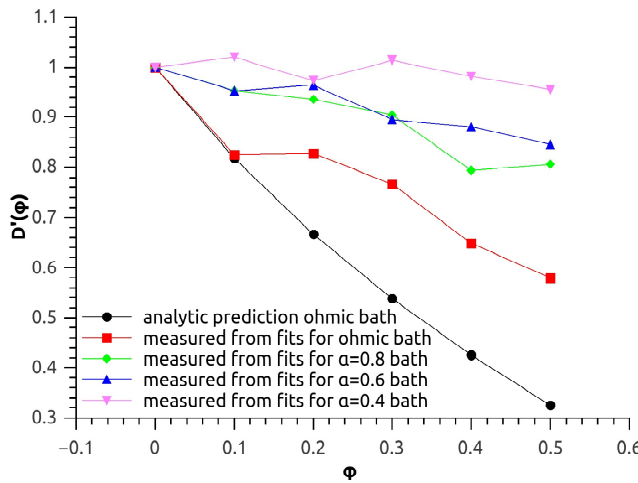
3.2 PARTICLE IN A 1-D BOX

We also want to check whether or not the system shows a long time behavior consistent with equilibrium statistics. In that case, the known

Figure 3.3: $\alpha = 0.8$ plots. Figure ref 3.4a shows the linear fits of the MSD curves versus time, figure 3.4b the relative (generalized) coefficients of diffusion



(a) MSD for different sphere concentrations ϕ together with linear fits for $\alpha = 0.8$. All simulations for 14k bath particles at 100K temperature. All times have been rescaled by the lattice scale time $t_E = 3000s$, all MSD by the squares lattice constant L^2 . shows the linear of the MSD versus time, figure 3.4b the generalized diffusion coefficients relative to coefficient of free diffusion.



(b) plot of relative coefficients of diffusion $D'(\phi) = \frac{D(\phi)}{D(0)}$ as functions of volume fraction ϕ . For comparison the ohmic behaviour of the coefficients both measured and according to equation 3.1 have been added. The bath α - bath size pairs used are $(0.8, 1k)$, $(0.6, 21k)$, $(0.4, 40k)$.

canonical ensemble is essentially an indicator function and hence an easy comparison case. The Box is modeled as a potential with associated box length L

$$\begin{aligned} U(x) &= \begin{cases} 0 & -\frac{L}{2} \leq x \leq \frac{L}{2} \\ \infty & \text{else} \end{cases} \\ p_{\text{equilibrium}}(x) &\propto e^{-\frac{U(x)}{kT}} \\ &= \begin{cases} 1 & \frac{L}{2} \leq x \leq \frac{L}{2} \\ 0 & \text{else} \end{cases} \end{aligned}$$

Where $p_{\text{equilibrium}}(x)$ is the probability density of the distinguished particle at thermal equilibrium

The box will be set with length L, the particle starting in the middle. The length is chosen similar to the lattice spacing in the sphere simulations, that is $t_E = 3000s$, $L^2 = \frac{2D_\alpha}{t_E}$ to measure the system behaviour far above the ballistic time scale. For measuring the probability density function, the box interval will be separated into 100 bins at different measurement times, and the number n_i of simulations with a particle in a specific bin numbered i divided by the number of simulations N_S will give the probability of finding a particle in the bin interval

$$p\left(-\frac{L}{2} + i \cdot \frac{L}{100} \leq x < -\frac{L}{2} + (i+1) \cdot \frac{L}{100}\right) = \frac{n_i}{N_S}$$

To ensure the interval probability distribution is smooth enough to approach the continuous distribution $p(x)$, we will run $N_S = 5000$ simulations.

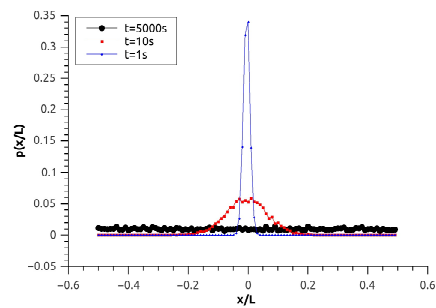
With these considerations out of the way, as per usual we start with the ohmic case and obtain figure 3.4

As we can see, the long term probability distribution indeed behaves as we expect $p_{\text{equilibrium}}(x)$ to. Now with the same parameter set ups we look at the sub-ohmic case

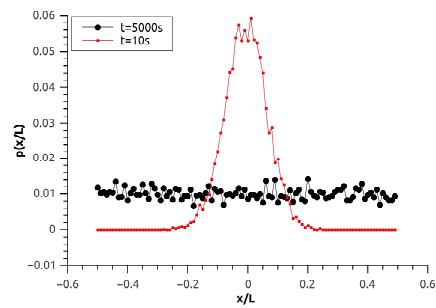
We see, that in all three sub-ohmic simulations, the equilibrium distribution is reached. Another feature on display is that the exponential distribution of the particle for small times becomes a stretched exponential for small $\alpha = 1$.

We then tried shrinking the box spacing L by powers of one half to show that these results stay consistent, the results are shown in figure 3.6.

Figure 3.4: Plot of the bin probabilities for $\alpha = 1$ rescaled by the box lengths L. figure 3.5a shows the behaviour at $t = 1s, 10s, 5000s$, figure 3.5b at only the later two times for better visibility.

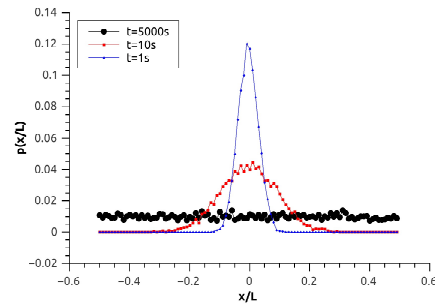


(a)

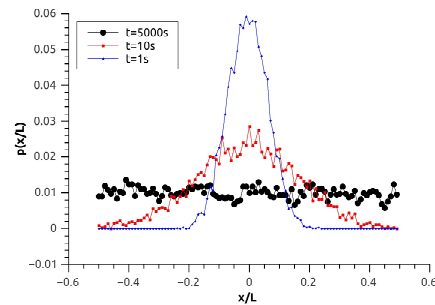


(b)

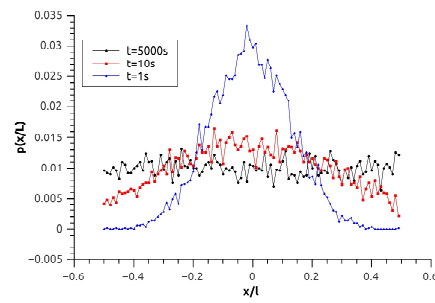
Figure 3.5: Plot of the bin probabilities in the sub-ohmic case rescaled by the box lengths L . figure 3.6a shows the behaviour at $t = 1s, 10s, 5000s$.



(a) $\alpha = 0.8$ plot



(b) $\alpha = 0.6$ plot



(c) $\alpha = 0.4$ plot

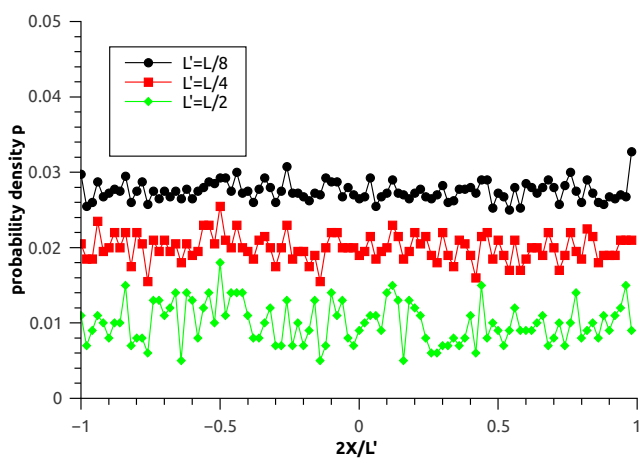


Figure 3.6: Plots of the probability density at simulation end for boxes of different lengths L' for $L' = \frac{L}{2}, \frac{L}{4}$ and $\frac{L}{8}$ compared to the length $L = 1.976 \cdot 10^{-2} \text{m}$, $t_E = 3000 \text{s}$ of the previous tests. $\alpha = 0.8$ and 14k bath particles, all other parameters are as in figure 3.5. The probability density for $L' = \frac{L}{4}$ and $\frac{L}{8}$ have been lifted upward by $\frac{1}{100}$ and $\frac{2}{100}$ for easier reading.

Part III
APPENDIX

BIBLIOGRAPHY

- [1] M. Abramowitz and I. Stegun. *Handbook of mathematical functions*. New York: Dover Publications Inc., 1970 (cit. on p. 18).
- [2] Fischer Black and Myron Scholes. "The Pricing of Options and Corporate Liabilities." In: *Journal of Political Economy* 81.3 (1973), pp. 637–654. DOI: [10.1086/260062](https://doi.org/10.1086/260062) (cit. on p. 3).
- [3] A. Einstein. "Zur Theorie der Brownschen Bewegung." In: *Annalen der Physik* 324.2 (1906), pp. 371–381. DOI: [10.1002/andp.19063240208](https://doi.org/10.1002/andp.19063240208). eprint: <https://onlinelibrary.wiley.com/doi/pdf/10.1002/andp.19063240208>. URL: <https://onlinelibrary.wiley.com/doi/abs/10.1002/andp.19063240208> (cit. on p. 3).
- [4] P.J. Flory. *Principles of Polymer Chemistry*. Cornell U. P., 1964. URL: <https://books.google.de/books?id=JFyetwEACAAJ> (cit. on p. 3).
- [5] Y.A. Houndonougbo, Brian Laird, and B.J. Leimkuhler. "A molecular dynamics algorithm for mixed hard-core/continuous potentials." In: *Molecular Physics* 98 (Mar. 2000), pp. 309–316. DOI: [10.1080/00268970009483294](https://doi.org/10.1080/00268970009483294) (cit. on p. 24).
- [6] Jae-Hyung Jeon and Ralf Metzler. "Fractional Brownian motion and motion governed by the fractional Langevin equation in confined geometries." In: *Phys. Rev. E* 81 (2 2010), p. 021103. DOI: [10.1103/PhysRevE.81.021103](https://doi.org/10.1103/PhysRevE.81.021103). URL: <https://link.aps.org/doi/10.1103/PhysRevE.81.021103> (cit. on p. 7).
- [7] K. Joseph, M. Ralf, and L.S. Cheng. *Fractional Dynamics: Recent Advances*. World Scientific Publishing Company, 2011. URL: <https://books.google.de/books?id=ECC7CgAAQBAJ> (cit. on p. 7).
- [8] R. Klages and Christoph Dellago. "Density-Dependent Diffusion in the Periodic Lorentz Gas." In: *Journal of Statistical Physics* 101.1 (2000), pp. 145–159. DOI: [10.1023/A:1026445601619](https://doi.org/10.1023/A:1026445601619). URL: <https://doi.org/10.1023/A:1026445601619> (cit. on p. 32).
- [9] R. Kupferman. "Fractional Kinetics in Kac Zwanzig Heat Bath Models." In: *Journal of Statistical Physics* 114 (Jan. 2004), pp. 291–326. DOI: [10.1023/B:JOSS.0000003113.22621.f0](https://doi.org/10.1023/B:JOSS.0000003113.22621.f0) (cit. on pp. 9, 10).
- [10] H. A. Lorentz. "The motion of electrons in metallic bodies I." In: *Koninklijke Nederlandse Akademie van Wetenschappen Proceedings Series B Physical Sciences* 7 (1904), pp. 438–453 (cit. on pp. 32, 35).

- [11] Jonathan Machta and Robert Zwanzig. "Diffusion in a Periodic Lorentz Gas." In: *Phys. Rev. Lett.* 50 (25 1983), pp. 1959–1962. DOI: [10.1103/PhysRevLett.50.1959](https://doi.org/10.1103/PhysRevLett.50.1959). URL: <https://link.aps.org/doi/10.1103/PhysRevLett.50.1959> (cit. on p. 32).
- [12] M. Sahimi. *Heterogeneous Materials I: Linear Transport and Optical Properties*. Interdisciplinary Applied Mathematics. Springer New York, 2003. URL: <https://books.google.de/books?id=z0FbntG6sNcC> (cit. on p. 36).
- [13] Christian Schmeltzer, Alexandre Hiroaki Kihara, Igor Michailovitsch Sokolov, and Sten Rüdiger. "Degree Correlations Optimize Neuronal Network Sensitivity to Sub-Threshold Stimuli." In: *PLOS ONE* 10.6 (June 2015), pp. 1–26. DOI: [10.1371/journal.pone.0121794](https://doi.org/10.1371/journal.pone.0121794). URL: <https://doi.org/10.1371/journal.pone.0121794> (cit. on p. 3).
- [14] M. V. Smoluchowski. "Über Brownsche Molekularbewegung unter Einwirkung äußerer Kräfte und deren Zusammenhang mit der verallgemeinerten Diffusionsgleichung." In: *Annalen der Physik* 353.24 (1916), pp. 1103–1112. DOI: [10.1002/andp.19163532408](https://doi.org/10.1002/andp.19163532408). eprint: <https://onlinelibrary.wiley.com/doi/pdf/10.1002/andp.19163532408>. URL: <https://onlinelibrary.wiley.com/doi/abs/10.1002/andp.19163532408> (cit. on p. 36).
- [15] Loup Verlet. "Computer "Experiments" on Classical Fluids. I. Thermodynamical Properties of Lennard-Jones Molecules." In: *Phys. Rev.* 159 (1 1967), pp. 98–103. DOI: [10.1103/PhysRev.159.98](https://doi.org/10.1103/PhysRev.159.98). URL: <https://link.aps.org/doi/10.1103/PhysRev.159.98> (cit. on p. 23).
- [16] D.J. Wright. "The digital simulation of stochastic differential equations." In: *Automatic Control, IEEE Transactions on* 19 (Mar. 1974), pp. 75 –76. DOI: [10.1109/TAC.1974.1100468](https://doi.org/10.1109/TAC.1974.1100468) (cit. on p. 3).
- [17] R. Zwanzig. *Nonequilibrium Statistical Mechanics*. Oxford University Press, 2001. URL: <https://books.google.de/books?id=4cI51360doMC> (cit. on pp. 6, 8, 9, 11).

COLOPHON

This document was typeset using `classicthesis` style developed by André Miede. The style was inspired by Robert Bringhurst's seminal book on typography "*The Elements of Typographic Style*". It is available for L^AT_EX and LyX at

<https://bitbucket.org/amiede/classicthesis/>

Final Version as of July 2, 2019 (`classicthesis` version 4.5).

SOFTWARE

All Fits have been done with QTIPLOT, version 0.9.8.9 , released under the terms of the GNU General Public License

The simulation itself has been implemented in C using the GNU SCIENTIFIC LIBRARY and parallelized via OpenMP. A skeleton variant of the implementation is hosted at

https://github.com/nowotnm/KAC_ZWANZIG_SIM

under the MIT public license.

Final Version as of July 2, 2019 (classictthesis version 4.5).

SELBSTÄNDIGKEITSERKLÄRUNG

Berlin, April 2019

Ich erkläre hiermit, dass ich die vorliegende Arbeit selbstständig verfasst und noch nicht für andere Prüfungen eingereicht habe. Sämtliche Quellen einschließlich Internetquellen, die unverändert oder abgewandelt wiedergegeben werden, insbesondere Quellen für Texte, Grafiken, Tabellen und Bilder, sind als solche kenntlich gemacht. Mir ist bekannt, dass bei Verstößen gegen diese Grundsätze ein Verfahren wegen Täuschungsversuchs bzw. Täuschung eingeleitet wird.

Berlin,

Maximilian Nowotnick